American Mineralogist, Volume 81, pages 119–125, 1996

Structural relationship between pyrite and marcasite

István Dódony,[1] Mihály Pósfai,[2,*] and Peter R. Buseck[2]

[1]Department of Mineralogy, Eötvös Loránd University, Budapest, Múzeum krt. 4/A, H-1088 Hungary
[2]Departments of Geology and Chemistry, Arizona State University, Box 871404, Tempe, Arizona 85287-1404, U.S.A.

Abstract

We studied pyrite spherules built of radiating crystals to establish the relationships among microstructure, composition, and macroscopic appearance. Results of high-resolution transmission electron microscopy (HRTEM) imaging and selected-area electron diffraction (SAED) show that many pyrite crystals contain planar faults perpendicular to one of the [001] axes. A comparison between HRTEM micrographs and images simulated for defect model structures indicates that the faults can be interpreted as single (101) layers of marcasite that disrupt the regular sequence of (002) layers in pyrite. Such a marcasite layer can be described as a boundary between two pyrite crystals that are related by a 2_1 screw axis parallel to [100]. Energy-dispersive X-ray spectrometry (EDS) indicates that such disordered pyrite crystals contain about 3 at% As. However, the distribution of As is uniform over heavily faulted and fault-free regions, indicating the As content is not related to the occurrence of marcasite lamellae in pyrite.

Introduction

Pyrite is the most abundant sulfide mineral; it is widespread in ore deposits and common in many sedimentary, metamorphic, and igneous rocks. It exhibits a range of interesting structural characteristics such as penetration twins, epitaxial inter- and overgrowths with its polymorph marcasite, and the occurrence of a variety of morphological types (Tokody 1952; Donnay et al. 1977; Bonev et al. 1985).

Pyrite and marcasite are polymorphs. Fe atoms are octahedrally coordinated in both structures. The octahedra share corners in pyrite, whereas in marcasite they share edges (Buerger 1931). Pyrite is cubic (a = 5.428 Å) with space group $Pa3$ (Bragg 1913; Finklea et al. 1976), whereas marcasite is orthorhombic (a = 4.443, b = 5.424, c = 3.387 Å) with space group $Pnnm$ (Buerger 1931; Brostigen et al. 1973; Tossell et al. 1981). A characteristic feature of both minerals is that S atoms form covalently bonded pairs.

The structural relationship between pyrite and marcasite has been discussed in several studies. Brostigen and Kjekshus (1970) proposed a hypothetical transformation of pyrite into marcasite through the reorientation of the S-S pairs. They noted that the pyrite {001} and the marcasite {101} planes show the same atomic arrangement. When epitaxial inter- and overgrowths of marcasite and pyrite occur, the two crystals commonly join in such a way that $\{001\}_{pyrite}$ is parallel to $(101)_{marcasite}$ with $\langle 100\rangle_{pyrite}$ parallel to $[010]_{marcasite}$ (Brock and Slater 1978; Gait and Dumka 1986). The same orientation relationship was found by Fleet (1970) in a study of the inversion of marcasite to pyrite.

TEM studies by Van Goethem et al. (1978), Fagot et al. (1978), and Fleet et al. (1989) showed that planar defects occur in pyrite parallel to {100}. The faults were interpreted by Van Goethem et al. (1978) as antiphase boundaries with a displacement vector ½[110]. Fagot et al. (1978) characterized the defects as stacking faults with $\mathbf{R} = \pm 0.29[010]$. However, Fayard et al. (1980) showed that the fault vector does not lie in the plane of the defect and identified it as $\mathbf{R} = a[0,0.27,0.5]$. They also mentioned that such faults produce a marcasite lamella in pyrite. A similar interpretation was given by Fleet et al. (1989) for the faults that they observed in pyrite. We found that none of these models correctly describes the marcasite-pyrite structural relationship; the defect structure produced by the $\mathbf{R} = a[0,0.27,0.5]$ displacement vector (Fayard et al. 1980) produces a structural unit that is similar but not identical to marcasite.

The goal of this study is to describe the geometry of the defects that we observed in disordered pyrite crystals. We interpret the faults on the basis of a new model for the marcasite-pyrite structural relationship and discuss the results of EDS analyses of faulted crystals.

Experimental methods

We studied pyrite samples from the Recsk porphyry copper ore deposit in Hungary. The ores occur in an Eocene subvolcanic andesite body that intruded Triassic carbonate rocks. Contact-metamorphic processes led to the formation of a 150–250 m thick mantlelike skarn zone around the intrusion (Morvai 1982). Pyrite formed during several stages of ore deposition; the hydrothermal

* Present address: Department of Mineralogy, University of Veszprém, P.O. Box 158, Veszprém H-8201, Hungary.

0003-004X/96/0102-0119$05.00

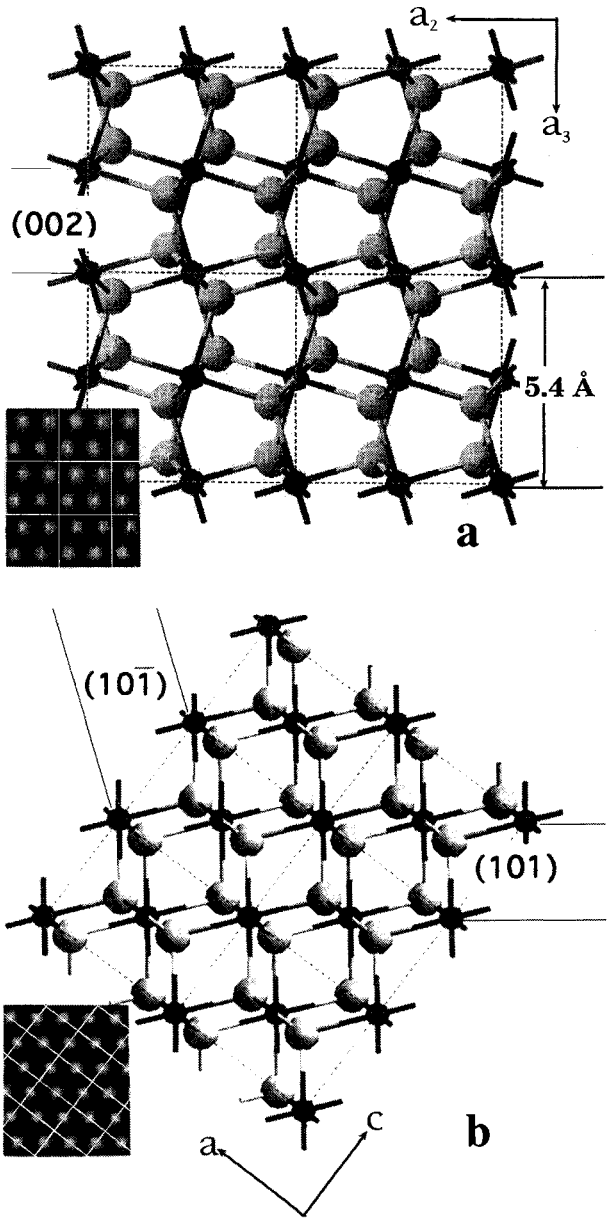

FIGURE 1. (a) The structure of pyrite, projected along [100]; (b) the structure of marcasite, projected along [010]. Fe atoms are dark spheres, S atoms are light spheres. The white regions in the simulated electron micrographs (lower left corners) are centered at the structural channels. The white lines define unit cells.

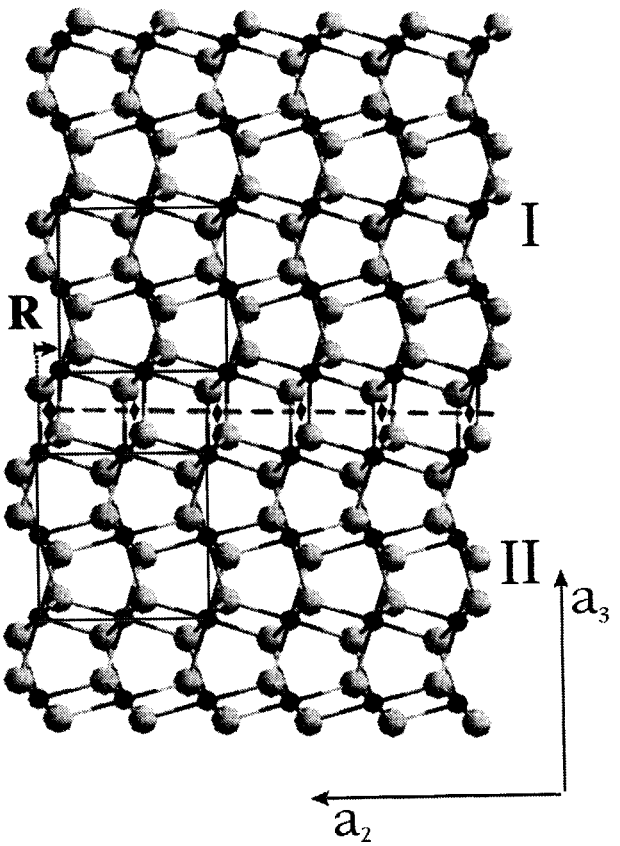

FIGURE 2. Model for a faulted pyrite structure. The fault plane is marked by the dashed line ([100] projection). The diamonds mark the positions of the 2_1 axes that are parallel to [100]. **R** denotes the projected displacement vector (**R** = 0.115[010]).

samples that we studied occur in lenses within the carbonate rocks, a few meters outward from the skarn zone.

The acicular, 2–4 mm long radiating crystals form small spherules. Pieces of the spherules were crushed under chloroform, and drops of the suspension were allowed to dry on holey carbon TEM grids. Ion-milled specimens were also prepared.

HRTEM images were obtained at 400 kV with a JEOL 4000EX transmission electron microscope equipped with a double-tilt goniometer stage ($x,y = \pm 25°$). Electron micrographs were simulated using Cerius software on a Silicon Graphics workstation; we processed and filtered digitized images using Gatan Digital Micrograph 2.1 on a Macintosh computer. Analytical electron microscopy was performed at 200 kV using a JEOL 2000FX electron microscope. We acquired EDS spectra with an ultra-thin-window Kevex X-ray detector and then processed and quantified them using the Quantex program. K factors for Fe and As were experimentally determined from As-free pyrite grains and arsenopyrite (FeAsS), respectively.

STRUCTURE MODEL

In the pyrite structure the S-S doublets are aligned parallel to the body diagonals of the cubic cell. If the structure is viewed along [100], the projected positions of the Fe atoms are at the centers of the S-S bonds (Fig. 1a). For this viewing direction the S-Fe-S triplets are alternately oriented in projected NE–SW and NW–SE directions along [001], whereas in rows parallel to [010] they all lie in either the SW–NE or the NW–SE direction.

The similarities and differences between the structures of pyrite and marcasite are best seen by comparing the [100] projection of pyrite with the [010] projection of mar-

casite (Fig. 1b). The two polymorphs share the same basic structural unit. A single S-Fe-S layer parallel to (101) in marcasite is identical to an S-Fe-S layer parallel to (00*l*) in pyrite. However, these basic layers are arranged according to a different scheme in the two structures. Instead of forming a zigzag pattern as in pyrite, all S-S doublets are parallel to one another in this projection of marcasite.

The computed HRTEM images in the lower left corners of Figures 1a and 1b were obtained at Scherzer defocus for 54 Å thick crystals. At these conditions the contrast in the micrographs is directly related to the structure. The white regions correspond to the channels between S-Fe-S triplets. The arrangements of the white spots in the two images reflect the difference between the stacking of S-Fe-S layers in pyrite and marcasite.

The pyrite-marcasite structural relationship can be described in terms of a pyrite structure that contains a planar fault (Fig. 2). In [100] projection, S-S pairs are oriented on both sides of the fault plane parallel to the two body diagonals in the $(0\bar{1}1)$ plane of pyrite, instead of lying alternately in the $(0\bar{1}1)$ and (011) planes. The centers of the S-S pairs (the Fe atoms) are shifted by 0.115 [010]. Such an arrangement occurs at the boundary of two pyrite crystals (I and II) that are brought into coincidence by a 2_1 screw axis parallel to [100], the direction of projection. The pair of S-Fe-S layers on the two sides of the boundary form a single $(10\bar{1})$ layer of marcasite (most easily seen when Fig. 1b is rotated clockwise by 90°).

Depending on its position relative to the pyrite unit cell, the 2_1 axis produces either a $(10\bar{1})$ or a (101) layer of marcasite. If the 2_1 axis occurs at $y = 0.135$, $z = 0.25$ (as marked in Fig. 2), the boundary structure is identical to a marcasite $(10\bar{1})$ layer; if it is at $y = -0.135$, $z = -0.25$, then a (101) layer of marcasite forms.

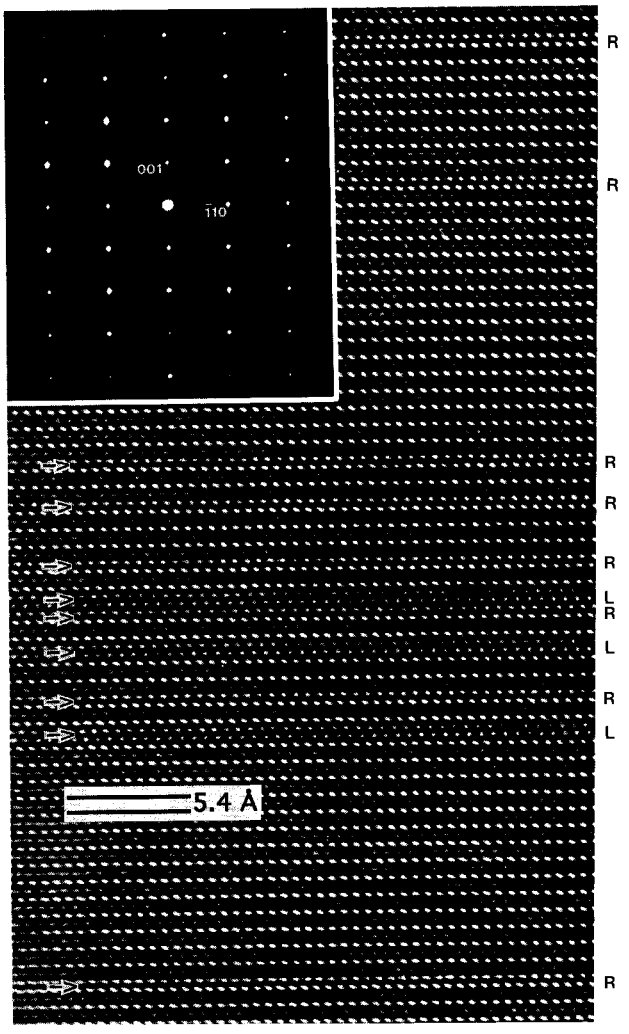

FIGURE 3. HRTEM image of a pyrite crystal ([110] projection) containing several single planar faults (marked by arrows). Faults occur with two orientations, marked L and R (see text).

RESULTS

Many pyrite crystals contain faults perpendicular to one of the ⟨001⟩ axes. The faults occur in bunches and result in a recognizable contrast change in HRTEM images obtained from ⟨100⟩- and ⟨110⟩-type directions (Fig. 3). The SAED pattern reveals that the faults are parallel to (001): There is faint continuous scattering parallel to [00*l*]* between reflections belonging to ordered pyrite. In the high-resolution image the stacking of (002) layers is changed by the defects, and two types of faults are distinguished. In fault-free regions of the crystal every second white spot along [001] is identically positioned; the faults introduce left (marked L) and right (marked R) sequences into the ordered stacking of (002) layers.

Figure 4A is an unprocessed, digitized micrograph, in [100] projection, of a pyrite crystal that contains two faults. The Fourier transform (FT) of the image shows diffuse intensity along the reciprocal lattice rows that are parallel to [00*l*]*. If the diffuse intensity in the FT is masked and only the pyrite reflections are used to construct Figure 4B, the contrast of the faulted region changes relative to Figure 4A. Figure 4C is produced by subtracting 4B from 4A. The only periodic pattern that can be observed appears at the fault. The FT of the boxed area in Figure 4C confirms that the diffuse intensity maxima between the pyrite reflections arise from the faulted region. [A discussion, with examples, of the manipulation of Fourier transforms is given by Buseck (1992, Figs. 1–6).]

When the pyrite reflections and the diffuse scattering contribute to the image but all the background intensity is filtered out (Fig. 4D), both the ordered pyrite regions and the faults appear with enhanced contrast. We produced Figure 4E by subtracting 4D from 4A. Only background noise appears, showing that all valuable information in the FT is contained within the reciprocal lattice rows that are parallel to [00*l*]*.

The pyrite crystal in Figure 5 contains both completely ordered and heavily faulted regions. In the SAED pattern there are diffuse spots between the pyrite reflections along the reciprocal lattice rows parallel to [00*l*]*, indicating

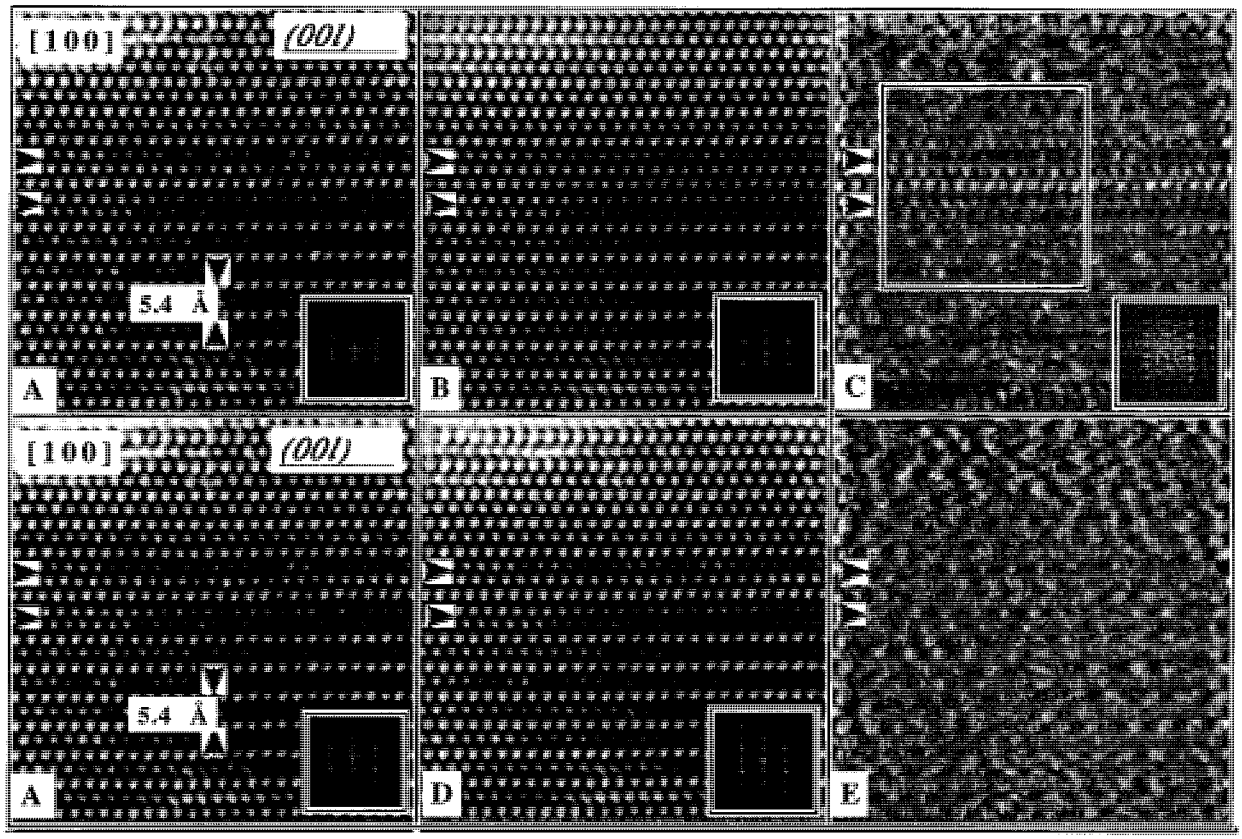

FIGURE 4. (A, top and bottom) Unprocessed, digitized images of a faulted crystal and its computed Fourier transform (inset). The faults are marked by arrows. (B) Filtered image of the area in A, produced by only the pyrite Bragg reflections. (C) The A − B subtraction results in an image that shows the nonpyrite part of the crystal. The inserted Fourier transform is calculated for the boxed area. (D) Reconstructed image produced by both pyrite and nonpyrite reflections. (E) The result of the A − D subtraction.

that the faults are oriented parallel to (00*l*) and perpendicular to those S-Fe-S layers in which the S-S bonds form a zigzag pattern. Therefore, the orientation of the faults is the same as in the structure model discussed above.

The high-resolution images shown in Figure 6 were obtained from the region marked AB in Figure 5. These structure images were interpreted on the basis of the pyrite-marcasite structural relationship described above. The model shown in the insert of Figure 6b was used to produce simulated images. We obtained a good match between calculated and experimental images (as seen in the lower right corner of Fig. 6a) and confirmed that the structural relationship between some adjacent S-Fe-S layers is the same as that between layers of marcasite (M), whereas other layer pairs are oriented as in pyrite (P) (Fig. 6b). As determined from high-resolution images, the M:P ratio is about 1:2 in the heavily faulted region AC of Figure 5.

The alternation of pyrite and marcasite structural units produces quasi-periodic sequences of S-Fe-S layers. At the bottom of Figures 6a and 6b there is a ten-layer band of marcasite. Elsewhere, in the disordered part of the crystal, both (10$\bar{1}$) and (101) layers of marcasite occur. Various layer sequences can be observed, with the four-layered PPPM unit appearing the most regularly. The presence of this variety of structural units gives rise to diffuse diffraction maxima along the [0*kl*]* ($k = 2n$) reciprocal lattice rows parallel to c^* (Fig. 5). The nonpyrite diffraction spots divide the spacings between pyrite reflections by nonintegral values.

The pyrite spherules contain up to 4.5 at% As. Because the structure of arsenopyrite is similar to that of marcasite, we hypothesized that As is contained in the structural defects or, at least, that the defects are associated with elevated As content.

We analyzed the crystal shown in Figure 5 using EDS. X-ray spectra were collected from the heavily faulted region AC and from areas of ordered pyrite on either side of AC. These analyses indicate that the distribution of As is uniform over the ordered and disordered regions. The crystal contains ~2.7 at% As, and the variation of the As concentration remains within the analytical error (±0.3 at%).

Discussion

The formation of structural defects in pyrite can be interpreted as either a growth phenomenon or a result of a marcasite → pyrite transformation. According to Murowchick (1992), pyrite formed by the inversion of marcasite can be recognized in polished section; it is anisotropic, contains numerous pores that form characteristic patterns, and in many places it consists of bundles of crystals in two distinct orientations relative to the marcasite parent. The structurally disordered pyrite from Recsk is optically anisotropic; however, neither pores nor two distinct pyrite orientations were observed. Therefore, accepting Murowchick's (1992) results, we conclude that the pyrite spherules are primary products of hydrothermal deposition and interpret the marcasite lamellae as growth defects.

The controlling mechanism of fault formation is unknown. Marcasite forms from acidic aqueous solutions (pH < 5) at low temperature (T < 240 °C), with $H_2S^0_2$ present at the site of deposition (Murowchick and Barnes 1986; Schoonen and Barnes 1991a, 1991b). It is possible that at the time of nucleation conditions episodically favored the formation of marcasite. Perhaps this is why the faults tend to concentrate into groups between ordered regions of pyrite.

We studied the relationship between macroscopic morphology and atomic structure by looking at ion-milled samples that were prepared to provide views from both the ends and the sides of pyrite fibers. Marcasite lamellae are abundant in images obtained from end-on views, whereas they seem much less common in images taken from directions perpendicular to the elongation direction of the crystals. It appears that the marcasite layers are oriented parallel to the directions in which the pyrite crystals grew most rapidly (along [100] of each crystal).

In many places the marcasite lamellae terminate at grain boundaries. Owing to the slight mismatch between the dimensions of the pyrite (002) and marcasite (101) layers (0.13% between $[100]_{pyrite}$ and $[010]_{marcasite}$ and 1.25% between $[010]_{pyrite}$ and $[101]_{marcasite}$ dimensions), strain can accumulate along a marcasite lamella. This strain is released by the formation of grain boundaries along the termination of sets of defects. In this way, the presence of a marcasite lamella in pyrite limits the growth of the crystal along the marcasite [101] axis, which is the direction of the larger mismatch between the two structural units. Hence, it is possible that the planar defects control the cross-sectional size of pyrite fibers and are responsible for the characteristic morphology of the pyrite spherules.

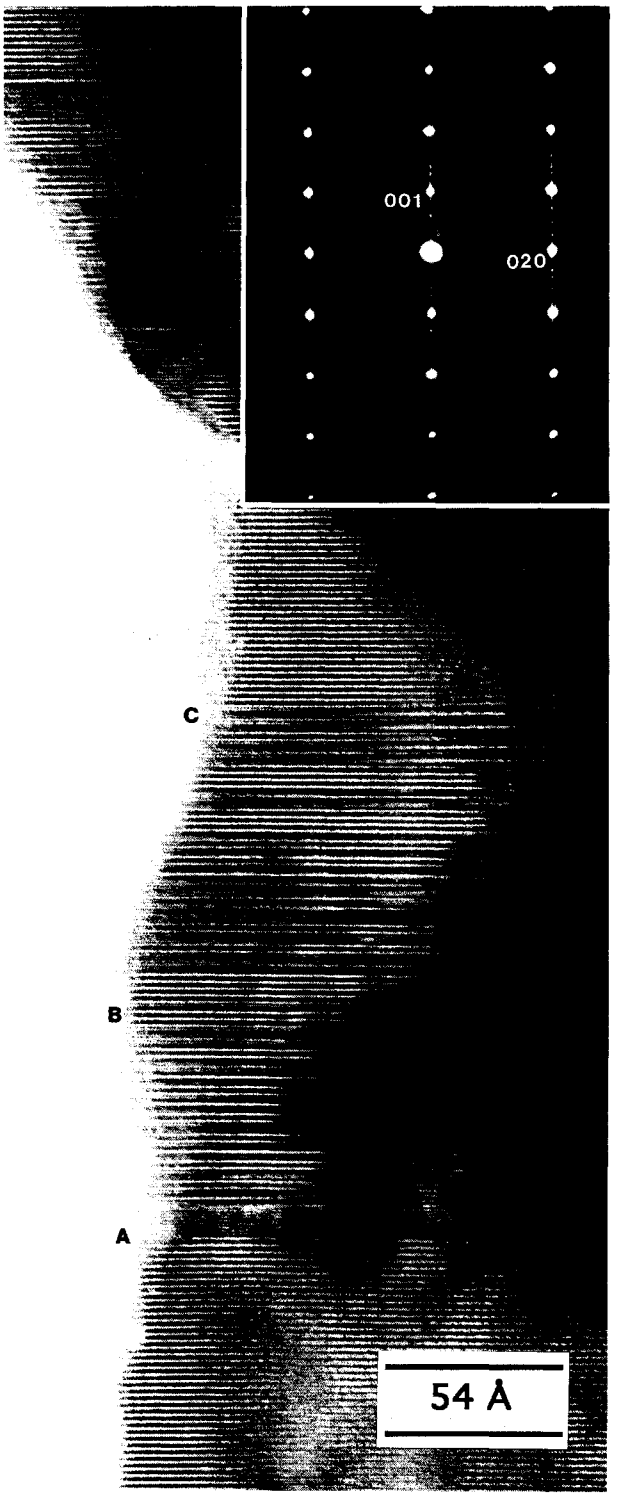

Figure 5. Low-magnification, [100] electron micrograph and SAED pattern of a pyrite crystal that contains both disordered and ordered regions (see text).

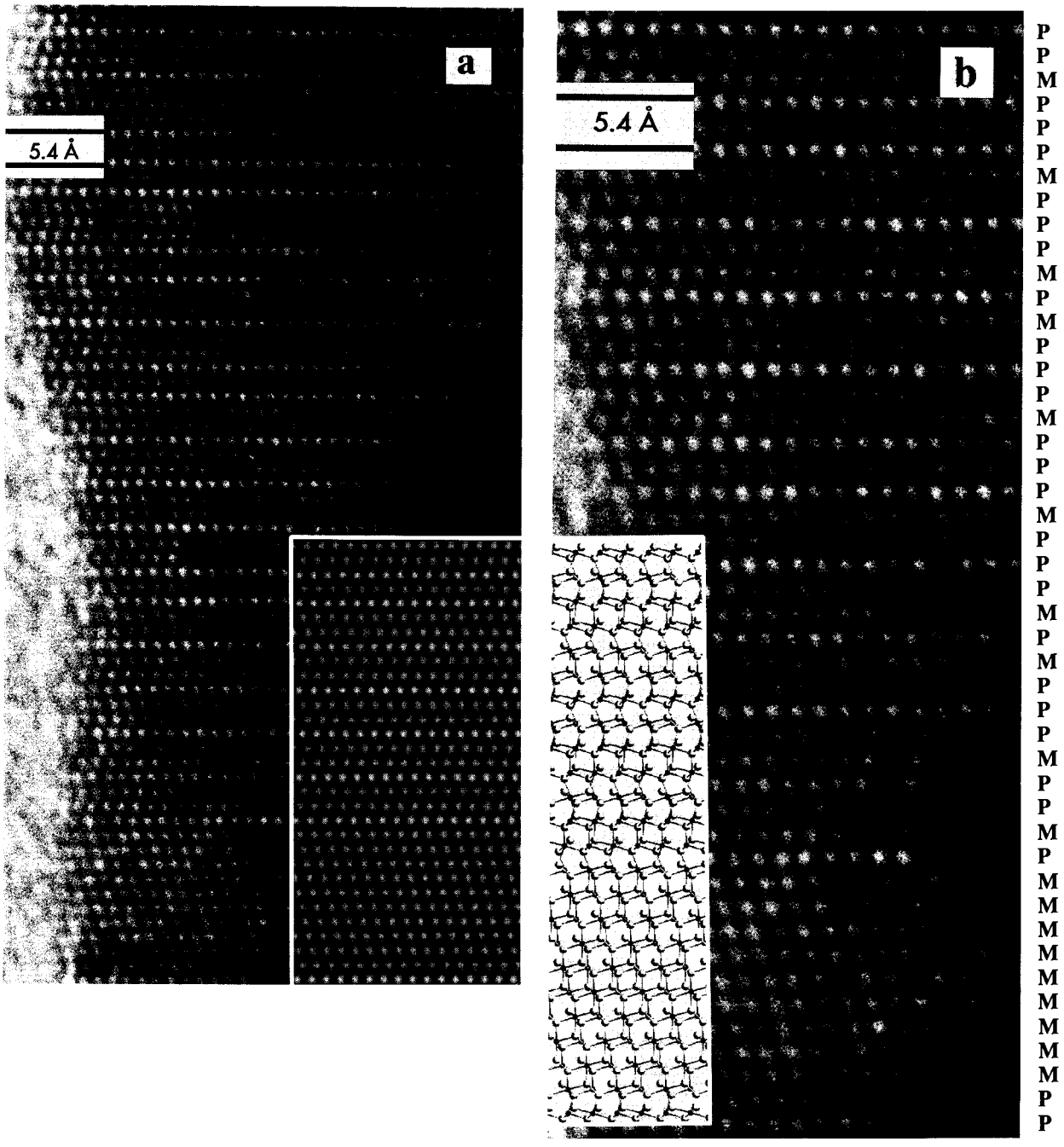

Figure 6. (**a**) Comparison between a simulated micrograph (lower right corner) and the experimental high-resolution image obtained from region AB of the crystal in Figure 5. The simulated micrograph was calculated for a 54 Å thick crystal at −500 Å defocus and 0.9 mrad beam tilt. (There is a slight mismatch between the experimental and simulated micrographs, produced by the process of model building. The model was constructed by cutting and pasting fragments of a pyrite structure; therefore, it cannot reproduce the small differences that exist between the corresponding dimensions in pyrite and marcasite slabs.) (**b**) Comparison between the structure model and the experimental image for the bottom part of region AB. M = marcasite, P = pyrite.

ACKNOWLEDGMENTS

We thank John Rakovan for calling our attention to some studies on the morphology of pyrite. Discussions with David Smith on the effects of beam misalignment in HRTEM are gratefully acknowledged. This study was supported by National Science Foundation (NSF) grant EAR-9219376 (to P.R.B.). We used TEMs located in the Center for High Resolution Electron Microscopy, which is supported by the National Science Foundation under grant no. DMR-8611609. I.D. was supported by Hungarian National Research Foundation (OTKA) grant T007545. We thank Bruce Hyde for his helpful comments.

REFERENCES CITED

Bonev, I.K., Reiche, M., and Marinov, M. (1985) Morphology, perfection and growth of natural pyrite whiskers and thin platelets. Physics and Chemistry of Minerals, 12, 223–232.

Bragg, W.L. (1913) The analysis of crystals by the X-ray spectrometer. Proceedings of the Royal Society of London, A89, 468–489.

Brock, K.J., and Slater, L.D. (1978) Epitaxial marcasite on pyrite from Rensselaer, Indiana. American Mineralogist, 63, 210–212.

Brostigen, G., and Kjekshus, A. (1970) On the relationships between the structure types pyrite, marcasite, and arsenopyrite. Acta Chemica Scandinavica, 24, 2983–2992.

Brostigen, G., Kjekshus, A., and Romming, C. (1973) Compounds with the marcasite type crystal structure: VIII. Redetermination of the prototype. Acta Chemica Scandinavica, 27, 2791–2796.

Buerger, M.J. (1931) The crystal structure of marcasite. American Mineralogist, 16, 361–395.

Buseck, P.R. (1992) Principles of transmission electron microscopy. In Mineralogical Society of America Reviews in Mineralogy, 27, 1–35.

Donnay, G., Donnay, J.D.H., and Iijima, S. (1977) A high-resolution electron micrograph of the twin boundary in pyrite. Acta Crystallographica, A33, 622–626.

Fagot, M., Levade, C., Couderc, J.-J., and Bras, J. (1978) Premières observations par microscopie électronique de défauts d'empilement dans la pyrite. Philosophical Magazine, A38, 353–358.

Fayard, M., Gratias, D., and Portier, R. (1980) Modèle de défaut d'empilement dans la pyrite. Philosophical Magazine, A41, 125–128.

Finklea, S.L., III, Cathey, L., and Amma, E.L. (1976) Investigation of the bonding mechanism in pyrite using the Mössbauer effect. Acta Crystallographica, A32, 529–537.

Fleet, M.E. (1970) Structural aspects of the marcasite-pyrite transformation. Canadian Mineralogist, 10, 225–231.

Fleet, M.E., MacLean, P.J., and Barbier, J. (1989) Oscillatory-zoned As-bearing pyrite from strata-bound and stratiform gold deposits: An indicator of ore-fluid evolution. Economic Geology Monograph, 6, 356–362.

Gait, R.I., and Dumka, D. (1986) Morphology of pyrite from the Nanisivik Mine, Baffin Island, Northwest Territories. Canadian Mineralogist, 24, 685–688.

Morvai, G. (1982) Hungary. In F.W. Dunning, W. Mykura, and D. Slater, Eds., Mineral deposits of Europe, p. 13–54. Mineralogical Society, London, U.K.

Murowchick, J.B. (1992) Marcasite inversion and the petrographic determination of pyrite ancestry. Economic Geology, 87, 1141–1152.

Murowchick, J.B., and Barnes, H.L. (1986) Marcasite precipitation from hydrothermal solutions. Geochimica et Cosmochimica Acta, 50, 2615–2629.

Schoonen, M.A.A., and Barnes, H.L. (1991a) Reactions forming pyrite and marcasite from solution: I. Nucleation of FeS_2 below 100 °C. Geochimica et Cosmochimica Acta, 55, 1495–1504.

——— (1991b) Mechanisms of pyrite and marcasite formation from solution: III. Hydrothermal processes. Geochimica et Cosmochimica Acta, 55, 3491–3504.

Tokody, L. (1952) Kristallographische Untersuchungen an Pyriten aus dem Karpatenbecken. Acta Geologica Academiae Scientiarum Hungaricae, 1, 327–339.

Tossell, J.A., Vaughan, D.J., and Burdett, J.K. (1981) Pyrite, marcasite and arsenopyrite type minerals: Crystal chemical and structural principles. Physics and Chemistry of Minerals, 7, 177–184.

Van Goethem, L., Van Landuyt, J., and Amelinckx, S. (1978) Study of the glide elements in pyrite by means of electron microscopy and electron diffraction. American Mineralogist, 63, 548–550.

MANUSCRIPT RECEIVED MARCH 16, 1995
MANUSCRIPT ACCEPTED AUGUST 31, 1995